Tellus (1999), 51A, 489–504
Printed in UK. All rights reserved

TELLUS
ISSN 0280–6495

Small-scale surface wind prediction using dynamic adaptation

By MARK ŽAGAR[1]* and JOŽE RAKOVEC[2], [1]*Hydrometeorological Institute of Slovenia, Ljubljana, Vojkova 1b, SI-1000 Ljubljana, Slovenia;* [2]*Faculty of Mathematics and Physics, University of Ljubljana, Jadranska 19, SI-1000 Ljubljana, Slovenia*

(Manuscript received 10 July 1998; in final form 12 March 1999)

ABSTRACT

An efficient method for surface wind prediction based on dynamic adaptation of a low-resolution model forecast towards a finer mesh is described. The method consists of: (1) interpolation of the data field predicted by the large-scale model onto the target grid; (2) dynamic adaptation of the fields onto the new grid by running the fine-mesh model for an appropriate period of time. The time necessary for the adaptation is roughly estimated by scale analysis and by using a linear model, and confirmed by some numerical simulations. This time was found to be between 30 and 45 min for adjusting general features of the wind field; the additional time needed to adjust small-scale wind phenomena can be several times longer. It was shown that this time period does not depend on the model configuration. The main advantage of the presented method is its low computational cost. The adaptation with a simplified model is capable of reproducing small-scale features in the wind field which develop due to the new orography in the fine grid. The method fails in cases of certain atmospheric conditions or a wrong large-scale forecast.

1. Introduction

Nowadays, numerical modeling for operational weather prediction covers a wide range of scales, down to about 10 km. The price and availability of the computational power needed when simulating the atmosphere at a horizontal resolution higher than this represent a huge obstacle. There are also theoretical considerations regarding limited mesoscale predictability, mainly concerning the parameterisation of convective processes (Pielke, 1984). Consequently, it is a matter of general interest to try different approaches for diminishing the cost of producing a forecast of certain meteorological parameters. The surface wind is surely the one which depends the most on the description of the topography in the model.

Especially in mountainous areas, such as the Alpine region, the surface wind prediction of operational models in many cases shows important deficiencies. These are mainly due to small-scale influences, conditioned by the details of topography which are not resolved at the scale of the models used. However, several studies have shown that it is possible to simulate local wind characteristics, such as the channeling and overturning of wind (e.g., Gross and Wippermann, 1987; Masson and Bougeault, 1996; Smedman et al., 1996).

In Section 2, a method for dynamic adaptation of a coarse resolution numerical atmospheric model forecast towards a finer mesh is described in detail. The time needed for adaptation is estimated by scale-analysis and by using a simple linear model. This estimate is tested by performing numerical simulations.

* Corresponding author.

In Section 3 the numerical procedure is described. An appropriate configuration for a high resolution surface wind prediction model is defined. The influence of the models' resolution and dimensions, and of the boundaries is discussed.

The results are presented and some uncertainties are discussed in Section 4. Focusing on the surface wind as the forecast field of interest, the advantages of the dynamic adaptation method for this particular purpose are shown. The surface wind forecast obtained by this method is compared to the reference forecast, obtained by running the full high resolution model in "operational" mode.

The dynamic adjustment process takes a presumably predictable amount of time. According to various authors, the state was considered balanced already after 1 h, using an iterative time integration scheme in a model with a horizontal resolution of several degrees (Fox-Rabinovitz, 1996), while in another study by Kurihara and Tuleya (1978), who imposed a strong constraint by keeping all fields except momentum constant throughout the initialisation, the planetary boundary layer structure was established only after about 24 h of integration. In our approach, the numerical model is simply allowed to run from the initial state for a time considerably longer than the one being estimated by scale analysis and by the linear model.

2. Description of the method

The idea of using dynamic adjustment for the purpose of model initialization is not a new one. It has already been widely studied by Kurihara and Tuleya (1978), Majewski (1985), Fox-Rabinovitz and Gross (1993), Fox-Rabinovitz (1996), and other authors, but it has not been proposed, as far as we know, that the adjusted field could be employed as a forecast field. However, there are apparently many reasons for trying it.

2.1. Interpolation, dynamic adaptation

First of all, the fields have to be interpolated on to the target fine grid. This process of interpolation from the coarser grid of the driving model towards the finer grid of the adaptation model does not bring any new information about atmospheric variables, at least not in our particular case. It only perturbs the fields, destroying the quasi-stationarity state. Details of the interpolation are given in Subsection 3.1.

The new orography is introduced into the model with finer resolution. The main effects as regards the relief — due to the poor smoothing resolution of the previous one — are that new valleys open, and the tops of the hills become higher. So wind may change in direction and in velocity. For low level winds the valleys as new openings are more important. For higher level winds the higher tops as new obstacles are more important. Higher level winds must decelerate and deviate around the new obstacles, while low level winds may accelerate along the newly opened valleys.

The adaptation of the model fields to these new relief characteristics is performed by running the model with the new, fine resolution. This model is a simplified one. Part of the physics is excluded, and, as wind is influenced by the new topography mainly in the lower part of the troposphere, the number of vertical levels is diminished in the upper troposphere. Further details are given in Subsection 3.2.

A desirable condition for dynamic adaptation to provide a reasonable surface wind forecast is the quasi-steadiness of the planetary boundary layer. In the case of an evolving situation on a synoptic scale, the adaptation process becomes over-driven by other effects (e.g., advance of a cold front) and we cannot say that the state after an otherwise sufficient adaptation time is really a quasi-balanced one. Of course on the other hand, it is not feasible to adjust the adaptation period every time, depending on the situation itself.

The only force in the horizontal direction, causing the movement of the air is the pressure gradient force. An analogy for illustration could be as follows: opening a new path through a relief is similar to opening windows (or the door) in a room. The non-balanced pressure (pressure gradient force) is the cause of the draught through the opened windows. Or, if the wind is blowing towards the opened window, some of it is also advected into the room (the effect of inertial, or advective forces).

2.2. The adaptation time estimated by scale analysis

Scale analysis is one of the tools to determine the required time of integration of the model (full system of equations, but simplified physics) to allow the fields to adapt to the new relief. Typically in the mesoscale and in similar cases to ours, the horizontal and vertical length scale are of the order $L \sim 5$ km and $H \sim 1$ km. Wind velocity is typically $U \sim 5$ m/s, while in cases without free convection close to the ground typical vertical velocity W is proportional to the horizontal one U and to the inclination of the slopes. For slopes with 10° inclination $W \sim 1$ m/s. The Coriolis parameter in mid-latitude is $f \sim 10^{-4}\,\mathrm{s}^{-1}$.

The first estimate is based on the time-scale τ of local wind change $\partial \boldsymbol{u}/\partial t$. Pielke (1984) explains that local time-scale τ in complicated terrain and in small scale is well approximated by $\tau \sim L/U$ due to the prevailing advective and internal gravity wave changes. So the first estimate of the time of adaptation is roughly

$$\tau \sim \frac{L}{U} \sim 1000\ \mathrm{s} \approx 15\ \mathrm{min}. \qquad (1)$$

The next step is the scale analysis of the horizontal equation of motion (3) to determine the importance of individual terms in this equation. Again following Pielke (1984), a typical horizontal temperature differences ΔT at these small dimensions can be used for evaluation of the magnitude of the pressure gradient force:

$$\left|\frac{1}{\rho}\frac{\partial p}{\partial x}\right| = \left|R\frac{\partial T}{\partial x}\right| \sim R\frac{\Delta T}{L}. \qquad (2)$$

Due to uncertainty regarding the magnitude of the driving effect from one location to the other, the value of $\Delta T/L$ can vary from approximately 0.1 K/5 km to approximately 1 K/5 km and thus the magnitude of the pressure gradient force may have a value between $6 \cdot 10^{-3}$ and $6 \cdot 10^{-2}\,\mathrm{ms}^{-2}$; we take the value $10^{-2}\,\mathrm{ms}^{-2}$ as a representative one for this consideration. To obtain the rough order of magnitude of the (turbulent) friction force, which is very important over rough terrain, the simple linearised Newtonian friction force $-k\boldsymbol{u}$ can be applied, using a value of $k \sim 5 \cdot 10^{-4}\,\mathrm{s}^{-1}$ from the research study on wind in valleys by Nickus and Vergeiner (1984). So the magnitude of the terms in the equation of motion are assessed as follows:

$$\begin{array}{ccccccccccccc}
\dfrac{\partial \boldsymbol{u}}{\partial t} & + & \boldsymbol{u}\cdot\nabla_{\mathrm{h}}\boldsymbol{u} & + & w\dfrac{\partial \boldsymbol{u}}{\partial z} & + & \dfrac{1}{\rho}\nabla_{\mathrm{h}}p & + & f\boldsymbol{k}\times\boldsymbol{u} & + & k\boldsymbol{u} & = & 0, \\
\dfrac{U^2}{L} & + & \dfrac{U^2}{L} & + & \dfrac{UW}{H} & + & \dfrac{R\Delta T}{L} & + & fU & + & kU & = & 0, \\
5\cdot 10^{-3} & & 5\cdot 10^{-3} & & 5\cdot 10^{-3} & & 10^{-2} & & 5\cdot 10^{-4} & & 2.5\cdot 10^{-3}\,\mathrm{ms}^{-2} & &
\end{array} \qquad (3)$$

Here subscript h denotes the horizontal gradient operator.

The term of the Coriolis force is about one order of magnitude smaller than the other terms at these horizontal scales and with the chosen wind velocity and hence can be neglected in this concept. This fact is proved by a pair of numerical simulations. Fig. 1 shows the simulated time evolution of the surface wind vector at one point in two applications of the same fine grid numerical model: with and without the Coriolis term in the equation of motion. Notice that the difference between them grows in time and reaches a significant value after 6 h, whereas within the first hour of the adaptation period, the Coriolis force does not contribute much to the deviation of the surface wind from its initial value. Therefore neglecting the Coriolis term is justified for the first hour or so of the adaptation.

2.3. *The adaptation time estimated by a linear model*

To estimate the time scale of adaptation, taking into account the prevailing forces which govern the process, a linearised model is used (so advection is not considered separately), neglecting the Coriolis force. At the very beginning, before the values are interpolated to the denser resolution, the flow is stationary. Close to the ground the pressure gradient force as a general driving force on the large-scale and the (linearised) friction force are approximately balanced:

$$\frac{\partial \boldsymbol{u}_0}{\partial t} = 0 = -\left(\frac{1}{\rho}\nabla_{\mathrm{h}}p\right)_0 - k\boldsymbol{u}_0. \qquad (4)$$

After the change of resolution and after the interpolation of the model variables into a finer grid the flow is no longer balanced:

$$\frac{\partial \boldsymbol{u}}{\partial t} = -\left(\frac{1}{\rho}\nabla_{\mathrm{h}}p\right) - k\boldsymbol{u} = -\boldsymbol{f}_{\mathrm{p}} - k\boldsymbol{u}. \qquad (5)$$

For brevity we use the symbol $\boldsymbol{f}_{\mathrm{p}}$ for the pressure gradient force. This force and the wind vector are

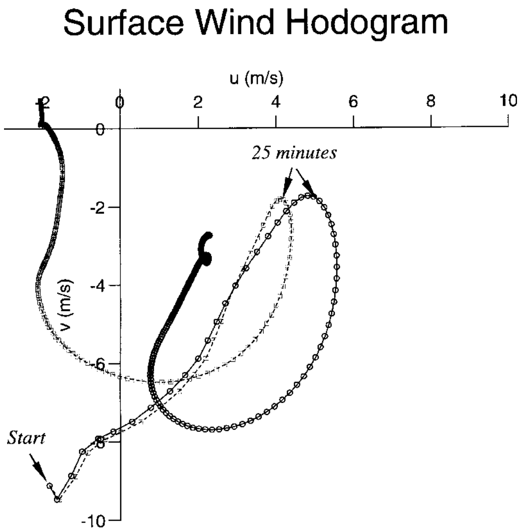

Fig. 1. Hodograms of surface wind at one point during 6 h of integration time. The simulation with the Coriolis force acting is plotted as a full line with circles at every minute and the one without the Coriolis force as a dashed line with boxes. It is necessary to mention that this point was chosen because of the large difference between the initial and final wind vector due to the fact that it lay inside a well pronounced and variable lee small-scale wind feature, so it does not represent an evolution during the adaptation period, typical of the whole area.

the combination of the large-scale ones ($\boldsymbol{f}_{p0}$ and $\boldsymbol{u}_0$) and of the perturbances caused by interpolation ($\boldsymbol{f}_{p'}$ and $\boldsymbol{u}'$); e.g., the force $\boldsymbol{f}_p = \boldsymbol{f}_{p0} + \boldsymbol{f}_{p'}$.

After the adaptation is finished, the flow is again stationary, but now with the two forces adapted: the balanced pressure gradient force and the friction force acting upon the adapted wind:

$$\frac{\partial \boldsymbol{u}_B}{\partial t} = -\left(\frac{1}{\rho}\nabla_h p\right)_B - k\boldsymbol{u}_B = -\boldsymbol{f}_{pB} - k\boldsymbol{u}_B. \quad (6)$$

Again the pressure gradient is a combination of the large-scale gradient, and the balanced small-scale pressure gradient force field, adapted to the relief: $\boldsymbol{f}_{pB} = \boldsymbol{f}_{p0} + \boldsymbol{f}_{pB'}$.

To see how the vector $\boldsymbol{u}$ changes in time towards the adapted, balanced value $\boldsymbol{u}_B$, a linearised model may be constructed by subtracting (6) from (5):

$$\frac{\partial(\boldsymbol{u} - \boldsymbol{u}_B)}{\partial t} + k(\boldsymbol{u} - \boldsymbol{u}_B) = -(\boldsymbol{f}_p - \boldsymbol{f}_{pB}). \quad (7)$$

It is not clear at this point how the difference of the two pressure gradient forces will behave in time. It is obvious that the difference diminishes in time as the pressure field approaches the balanced one. For simplicity we choose an analytical function for the decrease in time towards zero. An exponential decrease is somewhat arbitrary but perhaps the most natural choice:

$$|\boldsymbol{f}_p - \boldsymbol{f}_{pB}| \approx \Delta f_{p_0}\, e^{-t/\tau}, \quad (8)$$

where the initial value of the differences in pressure gradient forces is of the order of magnitude $\Delta f_{p0} \sim 10^{-2}\,\mathrm{ms}^{-2}$ and τ is the time scale we are trying to estimate. When a short notation is also applied for the magnitude of the velocity difference, i.e., $\Delta u = |\boldsymbol{u} - \boldsymbol{u}_B|$, the resulting scalar equation takes the form:

$$\frac{\partial \Delta u}{\partial t} + k\Delta u = -\Delta f_{p0}\, e^{-t/\tau}. \quad (9)$$

Integration of this equation offers a rough estimate of the necessary time needed to reach the new balance in the finer resolution of the model. Taking into account that the magnitude of the vector difference (Δu) diminishes as the wind approaches the balanced one, the solution of eq. (9) is:

$$\Delta u = \Delta u_0\, e^{-kt} - \left[\frac{\Delta f_{p0}}{(1/\tau) - k}\right](e^{-kt} - e^{-t/\tau}). \quad (10)$$

Using a linear approximation of the exponential function ($e^{-x} = 1 - x$), eq. (10) simplifies to the form:

$$\Delta u \approx \Delta u_0 - (\Delta f_{p0} + k\Delta u_0)t, \quad (11)$$

which is the same result as for the case of choosing a linear decrease of the magnitude of the difference in pressure gradient forces $|\boldsymbol{f}_p - \boldsymbol{f}_{pB}| \approx \Delta f_{p0}(1 - t/\tau)$, instead of exponential (8).

The time-scale of adaptation τ is the time in which a nearly balanced state is reached. With linear approximation of the pressure gradient forces difference τ is the time needed for Δu to approach 0 and in the exponential case towards the 1/e-th fraction of the initial value:

$$\tau \approx \frac{\Delta u_0}{\Delta f_{p0} + k\Delta u_0}. \quad (12)$$

With $\Delta f_{p0} \sim 10^{-2}\,\mathrm{ms}^{-2}$, $\Delta u_0 \sim 5\,\mathrm{ms}^{-1}$, and as has been already explained, $k \sim 5 \cdot 10^{-4}\,\mathrm{s}^{-1}$, another estimation of the adaptation time follows and with it the minimum time to run the model to reach the adapted state:

$$\tau \approx 400\,\mathrm{s} \approx 7\,\mathrm{min}. \quad (13)$$

Considering the relative importance of gradient and friction forces, the effect on adaptation time (eq. (12)) can be transformed into:

$$\tau^{-1} \approx \frac{\Delta f_{p0}}{\Delta u_0} + k. \tag{14}$$

The adaptation by friction (second term) is obviously much slower than adaptation due to the pressure gradient force.

When the pressure gradient force plays an important role (when a high pressure drag has to be relaxed), the time scale is rather small, approximately half the one, estimated by scale analysis in the previous subsection. Only when the pressure field contributes little to the adaptation process, does frictional dumping prevail and determines the time scale of adaptation. This is the case when the mountains in the (previous) coarse resolution do not cause much mountain drag and accordingly there is not much dynamic pressure to be relaxed when new paths open through the new valleys of the finer resolution. In this case, the time scale of the adaptation process by friction is approximately

$$\tau \approx \frac{1}{k} \approx 2000 \text{ s} \approx 30 \text{ min}. \tag{15}$$

Model integration for a period of 30 min should in most cases offer enough time for adaptation of the wind and mass field. Validation of this estimation with numerical experiments is presented in Subsection 4.2.

An additional illustration of the adaptation time is given in Section 7, with the time evolution of a water surface when one side of an infinite tank suddenly opens; similar to the case of a cool air pool in a basin when a new valley opens through the mountain ridge when finer resolution is applied.

3. Numerical procedure

The aim is to show that interpolation of the forecast wind field onto a finer grid and dynamic adaptation with a numerical model can serve as an appropriate method for obtaining a reasonable low-level wind forecast in a computationally effective and transparent way.

The simulations used for this study were performed using the Aladin spectral limited area model (more details in Horanyi et al., 1996). Aladin is the limited area version of the operationally running Arpege/IFS global model of Météo-France and ECMWF. It is a primitive equation model with a hybrid-η vertical coordinate (Simmons and Burridge, 1981). In this limited area model fields in spectral space are obtained by double Fourier transform and the periodicity condition is satisfied by adding to the computational domain a meteorologically meaningless extension zone in which the model variables are defined in such a way to make them biperiodic (periodic in both directions, Machenhauer and Haugen, 1987). Large-scale forcing (Davies, 1976) is imposed in the so-called coupling zone, being a four points wide outer belt of computational domain. At the outermost points, the values of variables are taken from the large-scale model and a polynomial relaxation function is used to combine the values from the large-scale model and the adaptation model inside the coupling zone.

3.1. *The interpolation*

The procedure of dynamic adaptation begins with an output of the numerical model (driving model); in the present study it is the Arpege/IFS global model. The horizontal resolution of this model over the area of interest (Fig. 2) is around 27 km. These data, containing the model variables, are then interpolated onto the grid of the adaptation model, where the orography representation already suits the increased horizontal resolution. The interpolation is done in several steps. First the model levels are defined, which follow the new orography. Then meteorological variables are horizontally interpolated from the coarse towards the dense grid, using bilinear operators. Vertical interpolation follows. Where levels in the adaptation model lie below the lowest level of the driving model, the values are extrapolated downwards. Extrapolation assumes a standard atmospheric gradient for temperature, while in the case of wind the value from the lowest level in the driving model is prescribed. By this interpolation fields in the computational space of the adaptation are defined and thus the initial conditions for the time integration.

3.2. *The adaptational model*

For the purpose of pointing out different issues in the dynamic adaptation approach for surface

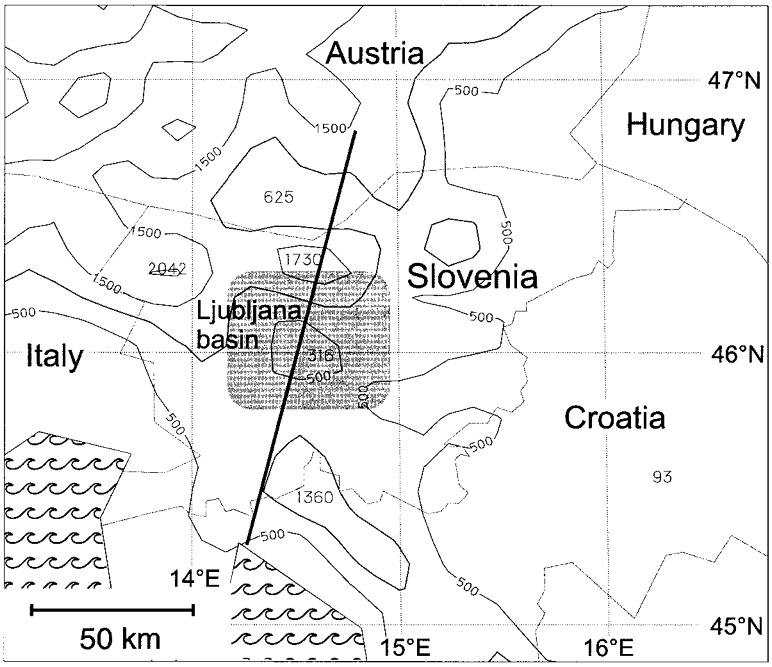

Fig. 2. Area of general interest (northern Adriatic and south-eastern flank of the Alps) with height contours depicted in 500 m intervals and with the shaded region representing the domain of particular interest. The line represents the direction of a vertical cross-section of Fig. 3b.

wind prediction, different computational domains are chosen.

The reference simulation R is a 6-h forecast with the full model (full vertical resolution with 27 levels, full physics) with a fine grid of 10 km horizontal resolution over a 510 km × 510 km area; this is approximately four times greater than the area shown in Fig. 2. The other domains correspond to the simplified adaptational model. They all cover the territory of central Slovenia but some are more and others less extended beyond the domain of particular interest, the Ljubljana basin. This is a flat bottomed valley at 300 m above mean sea level, around 30 km in diameter (shadowed in Fig. 2) and bounded on the northern side by a ridge of mountains of average height of 2000 m and maximum height of 2500 m, and separated from the Mediterranean by the Alpine-Dinaric ridge of 1000 m to 1500 m height. The model's horizontal resolution also varies from one configuration to another. The main characteristics of all the model configurations are given in Table 1.

Table 1. *Characteristics of the domains used*

Name	dx	No. points
R	10 km	51 × 51
S	10 km	23 × 23
M	10 km	51 × 51
L	10 km	71 × 71
F	5 km	45 × 45
VF	2.5 km	91 × 91

In all cases the central point of the domain is at 46°N and 14°30′E. The time-step during integration is the same for all cases (60 s). Configuration names reflect their basic characteristic. Reference R is the one with the full model (original number of 27 vertical levels and full physics). Adaptational models (reduced number of 14 vertical levels, simplified physics): S–small, M–medium, L–large, F–finer resolution, VF–very fine resolution.

Configurations S, M and L (small, medium and large) provide a framework for defining the optimal, or minimal size of the model domain.

They all have the same horizontal resolution of 10 km and vary only in the number of grid-points.

Configurations F and VF (fine and very fine resolution) are added to show the effect of more detailed topography and their purpose is to investigate further if some conclusions may be drawn from the experiments performed on a higher resolution such as 5 km and 2.5 km, and also whether the time needed for adaptation depends on the horizontal resolution.

Vertical discretization is the same in all adaptational models. From 27 model levels in the driving model and in the reference model R, 14 were kept in the adaptational models. The original density of model levels was retained in the lower troposphere in comparison to the full (or driving) model and to the reference model R, but at higher altitudes, they were much coarser. A sensitivity experiment revealed that the results of dynamic adaptation are not influenced by the reduced number of model levels in such a manner.

The package of physical parameterisations was also reduced. Since the time-scale of physical processes (such as condensation of water vapour inside a cloud layer, formation of precipitation, temperature changes due to radiation, etc.) is much longer than that of dynamic adjustment of wind, this part of the parameterisations was omitted in adaptation simulations. By doing this, we consciously sacrifice part of the model's ability in favour of cheaper computation. Hence the dynamic adaptation approach for small-scale wind forecasting cannot predict such phenomena as local thermal circulation, for example.

The reference model R was run for the prognostic range of 6 h, when the adaptational models start; for these models this was time 0 h in Figs. 6, etc. Adaptational models were run for next couple of hours (up to 6 h ahead) towards the stationary state. So, the values of adaptational models should be compared to the final field of the reference model R. In order to assure a high degree of stationarity inside the adaptation period, the boundary conditions for the adaptational model integrations were kept constant in our numerical experiments, meaning that the model was coupled with the same large-scale solution at every time-step.

It should be mentioned that the method may be applied exactly in the same way, in the case when the initial data are taken from the output of any limited area model instead of a global one.

3.3. The selected case

For the evaluation of the method, a quasi-stationary case is the most appropriate. The situation on 20 November 1995, was characterized by a strong northern flow in the area of the eastern Alps (Fig. 3a), causing very strong winds of northerly directions at the surface. In such a situation, the *föhn* effect is common in the lee of the mountains, as in the case of the Ljubljana basin. The lee effects in the wind field may appear under these circumstances at the downwind side of the mountain ridge. The case is also chosen because of the almost neutral stratification of the atmosphere (Fig. 3b), without the appearance of stable or unstable layers of any types. The dynamic adaptation clearly cannot result in a good surface wind forecast if in reality an inversion exists, for instance, which was not resolved at the scale of the driving model, or, as most of the physics is excluded, convection in an unstable atmosphere. So the fact that the lower troposphere was well-mixed is also of advantage in this example.

4. Results and discussion

As already mentioned, the reference experiment was performed with the full model's 6-h forecast. The result (Fig. 4b) is supposed to represent the actual development at a 10 km resolution. Comparison with the large-scale field (Fig. 4a) shows that with fine resolution adaptation the wind field changes and many small-scale features are simulated. Other adaptational experiments were compared with this reference and between themselves.

4.1. Influence of the size of the domain

Considering the demanded computational effectiveness of the method, the first question that arises is how small the computational domain may be to prevent the large-scale solution from spreading from the borders throughout the domain. The domain should also enable the development of small-scale phenomena, such as rotors and channelling, calms in the lee of mountains

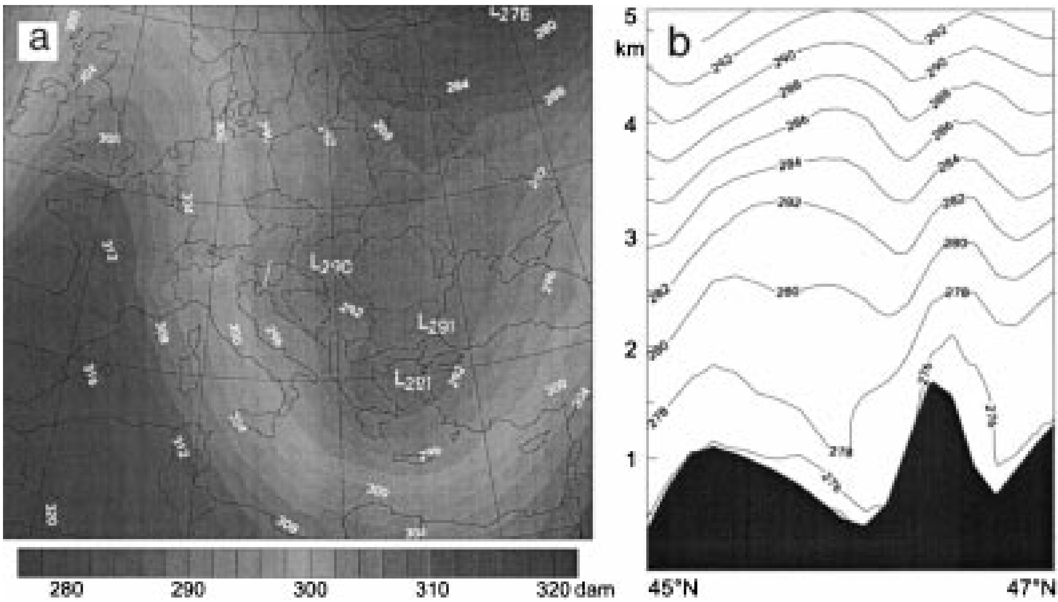

Fig. 3. 700 hPa geopotential on 20 November 1995 at 12 UTC (a) and the potential temperature on the cross-section above the Ljubljana basin (b) over the baseline seen on Figure 2.

and their persistence for longer periods of time. The way to identify the appropriate size of the domain is to compare the results of three different configurations of the adaptation model, namely S, M and L (small, medium, large) with the reference R, and between themselves. The only difference between domains S, M, and L is the horizontal size of the domain.

A characteristic feature to lean on, a relatively calm area in the lee of the mountains (Figs. 4b,c), was provided by the situation itself. Measurements also indicate the appearance of such wind feature in nature for the chosen case.

4.1.1. Qualitative comparison of wind fields. The initial state, that is the wind field interpolated from the 27 km grid of the driving model on to the 10 km grid, is shown in Fig. 4a. Fig. 4b shows the 10 m wind field after 6 h of simulation over the medium-size domain using the full, reference model R, that is with a complete package of physical parameterisations and the original number of levels and in the same high resolution (10 km). It is evident that the relative lee calm develops in the case of this full model forecast and this figure basically represents the goal forecast for this adaptation experiment. In this article a great deal of attention is paid to the study of the behavior of this particular new small-scale phenomenon of the fine grid under different model set-ups.

How successful are configurations S, M and L in simulating this particular feature of the wind field? The relative calm in the horizontal wind field, and a three-dimensional vortex connected with it at the northern edge of the shaded area in Fig. 2, has appeared in all configurations after 20 min of integration. However, in the simulation using the smallest domain (S, Fig. 4d) it decays soon after, while in the set-ups where the domain of particular interest is further from the edge of the model (M and L), this vortex persists: the result of model M is presented in Fig. 4c.

4.1.2. Quantitative comparison in a single point. To compare the conduct of different domains quantitatively, the time evolution of the v-component of the wind at one point in the area of the lee calm was studied. The points are approximately at the same geographical location in the model space of all domains, but due to the different model geometry and representation of topography not all of the five chosen points effectively describe exactly

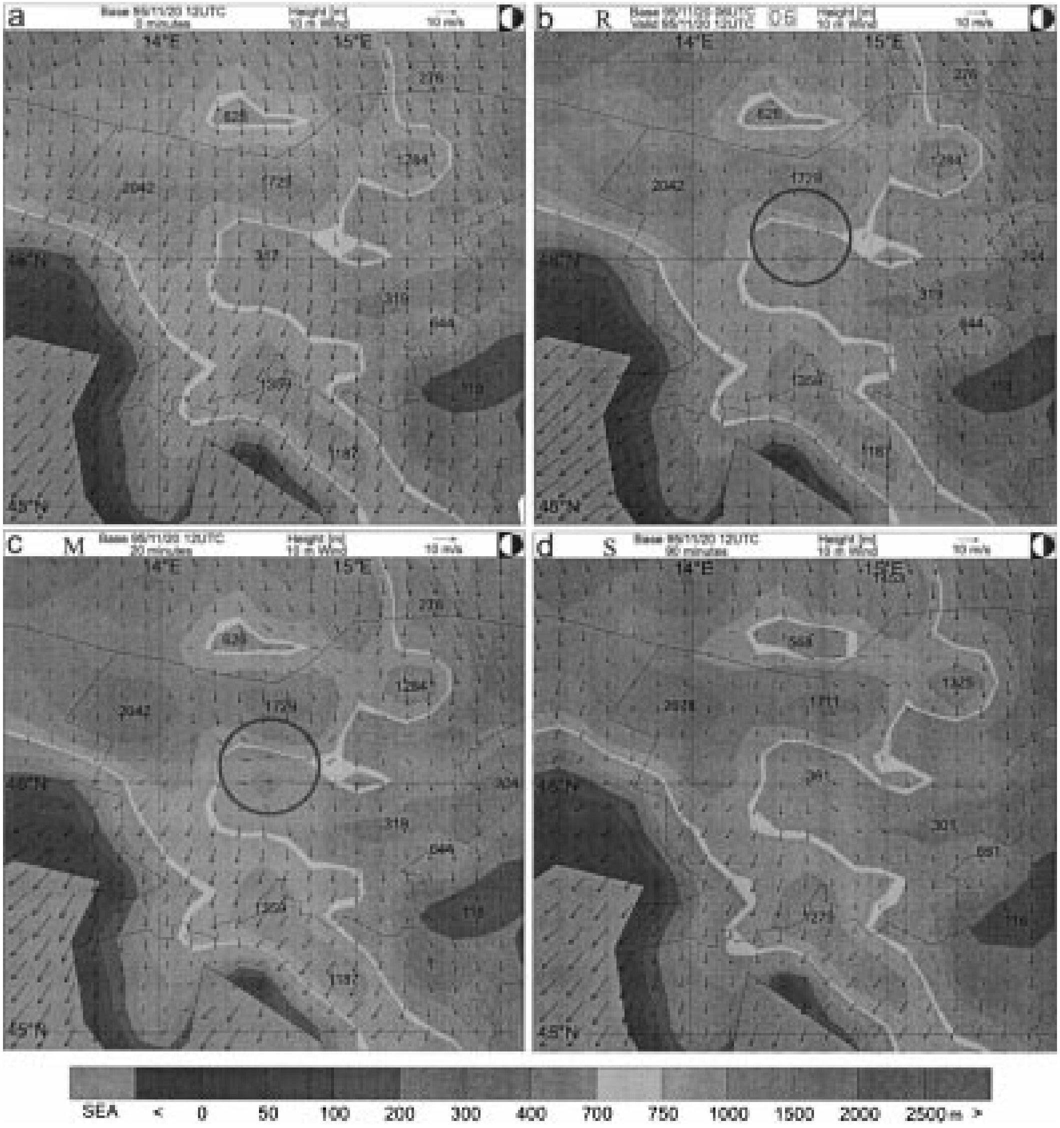

Fig. 4. 10 m wind field over central and western Slovenia. (a) Initial interpolated wind; (b) 6 h forecast of configuration R; run in operational mode; (c) after 20 min of integration of configuration M; (d) after 90 min of integration of configuration S. In plates (b) and (c), the region of relative lee calm is denoted by a circle. Note: (a), (b) and (c) show a zoom from domain M(R) to domain S (d).

the same geographical position in nature; see Fig. 5.

The time evolution of the v-component of the surface wind at the points mentioned is shown in Fig. 6. At the beginning there is a north wind ($v \sim -9$ m/s), which, during simulation with the denser grid models, changes due to the development of the lee calm.

To repeat: the reference model R was run for the prognostic range of 6 h, when the adaptational models started. So, the values of the adaptational models should be compared to the final field of

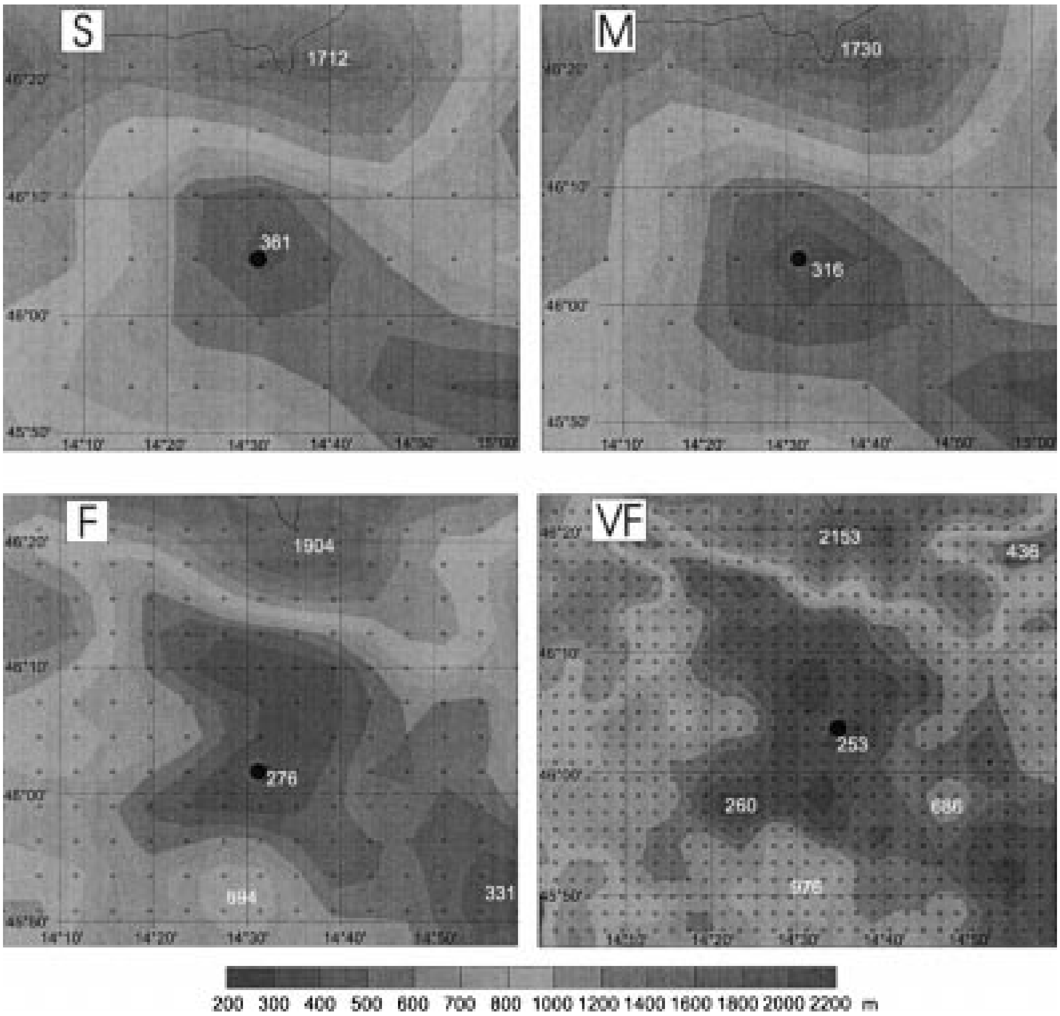

Fig. 5. Resolution and position of grid-points of different configurations of adaptational models over the area of special interest (the shaded region in Fig. 2). The large black dot represents the point where the time evolution of surface wind was investigated.

the reference model R. As regards the v-component at the point of the relative lee calm, the reference model R offers the quasi-stationary value of -2.7 m/s, represented by a black dot in Fig. 6. We say quasi-stationary because of the fact that inside the last half an hour before the initial time of the adaptational models, this value slightly oscillated, indicating that the vortex changes in time.

The time change of the v-component also gives a clue about the insufficient size of domain S, considering the fact that after an initial shock the value returns monotonously towards the quasi-balance of ~ -6 m/s. This quasi-balance in domain S also does not differ from the initial value as much as in the case of the two other larger domains M and L. In the case of domains M and L the adaptation after 60 and 90 min re-establishes a relative calm in spite of large-scale forcing. The large-scale forcing is due to the influence of the boundaries, tending to make the northerly wind prevail over the whole domain. So

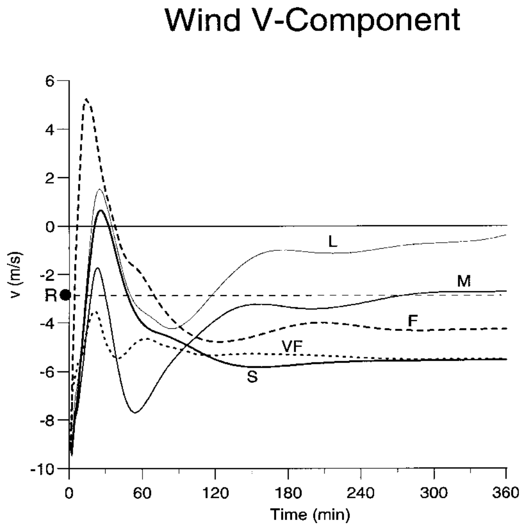

Fig. 6. Time evolution of the v-component of surface wind at the lowest point of the Ljubljana basin. Full lines (heavy, medium and light) represent configurations with the same resolution and the thick lines (full, long- and short-dashed) configurations with the same size of domain. The large dot and the thin dashed line represent the value from the quasi-stationary state of the reference model.

we may conclude that the domain M (51×51 points) is already big enough to reproduce this particular small-scale phenomenon.

Whether it is the physical distance from the border or the numerical distance — the number of points — that determines the sufficient size of the modelling domain in which small-scale features (like calms, rotors and channelling) may persist for a longer time period can be assessed by studying Fig. 6 carefully. First we compare the signatures of experiments M and F (reminder: the same number of points, different size). The fact that for F the value of the v-component of the surface wind drops monotonously after an initial shock which is not the case for M, makes us believe that it is the physical distance from the border and not the number of points that plays the major role in the conduct of the adaptation process. This can be further confirmed by comparing the curves for S and F, where the different number of points in the equally-sized domain does not significantly change the evolution of the wind over the point.

The VF experiment (very fine resolution, but only on a small domain, Fig. 6) offers similar results as the S experiment, due to the fact that the domain is the same and too small.

4.1.3. Quantitative comparison of domain averages. As already mentioned; the single points of comparison are at approximately the same geographical location in the model space of all domains, but due to the different model geometry and representation of topography not all of the five chosen points effectively describe exactly the same geographical position in nature. This is the reason for not only comparing single points but also performing area averaging for purposes of quantitative comparison. In averaging positive and negative differences partly cancel, so the comparison is done for domain averages of absolute vector difference between the actual and the initial wind (Fig. 7). The area average in the reference model R is 2.75 m/s of deviation from the initial state of the adaptational model M. For comparison the same absolute difference is plotted for solution of the analytical linear model (friction-like adaptation): $\partial u/\partial t = -k(u - u_B)$, $k = 2 \cdot 10^{-3}\ s^{-1}$, $u_0 = 0$, $u_B = 3$ m/s. Fig. 7 shows that all models, even the

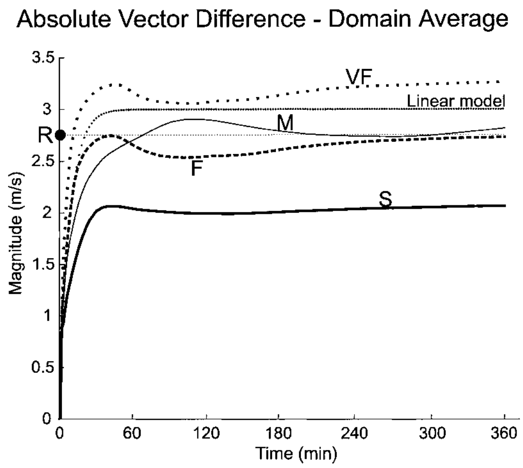

Fig. 7. Time evolution of the absolute vector difference $|\boldsymbol{u} - \boldsymbol{u}_0|$, averaged over the whole domain. Full lines (heavy and light) represent configurations with the same resolution and thick lines (full, long- and short-dashed) configurations with the same size of domain. Small circles represent the solution of the linear model ($\partial u/\partial t = -k(u - u_B)$, $k = 2 \cdot 10^{-3}\ s^{-1}$, $u_0 = 0$, $u_B = 3$ m/s). The large dot and the thin dashed line represent the value from the quasi-stationary state of the reference model.

linear approximation, behave similarly to the reference model R, except to some extent the model S on the obviously too small domain.

Looking at the results of the VF experiment (very fine resolution), one may notice that when the change of resolution from the coarse one of the driving model to the finer one of the adaptational model is larger, the adaptation forcing becomes stronger. In the VF experiment, although it is run on an equally small area as the S model, the forcing just appears to be strong enough to even counteract the effects from the nearby borders, thus retaining some local, small-scale features in the wind field (some, but not all; see the reasoning at the end of Subsection 4.1.2).

4.2. *Duration of the adaptation period*

Apart from the result of scale analysis and the linear model, there is no objective measure to estimate the necessary duration of the adaptation period in numerical simulations. But we may draw a conclusion from the results we have at hand (two-dimensional fields or time-evolution plots of point values and area averages). Here a few instructive examples are shown.

From the Fig. 7 it seems that it is proper to estimate the length of the adaptation period at 30–45 min, if one is interested in the general situation over the whole area. Most of the adjustment towards the balanced state happens within this period. In the same time period, the analytical solution obtained from the linear model seems to match well enough the numerical solution. However, in some specific points with strong, local wind modifications (like that of the three-dimensional vortex, connected to the lee calm, Fig. 6), this time could be considerably longer.

We have already asked the question whether the duration of the adaptation period depends on the model configuration or not. Judging from Fig. 7 the answer could be negative. The explanation of differences between the signatures of the S, F and VF experiments (same size of domain, different resolution) is straightforward. As the resolution increases, more and more valleys open. There are more and more local effects and so the average deviation of the adapted wind from the initial state is bigger.

It is also interesting to make sure of what is the actual role of numerical mechanisms versus real atmospheric dynamics in the process of dynamic adaptation. For this purpose another integration was performed but with a time-step twice shorter (30 s). A very clear conclusion can be drawn and it suffices to compare Fig. 8. If only the real time was important, then the full and the dashed line in Fig. 8a would overlap (and actually we can see this is the case). In the totally opposite case, if only the number of time-steps mattered, the lines in Fig. 8b would overlap. Therefore one very important conclusion can be drawn, that the dynamic adaptation, as it is performed in this study, is a purely dynamic and not a numerical process. Consequently, this encourages the assumption that the method is not model-dependent and may therefore be used widely.

4.3. *Which processes disable successful adaptation?*

The aim of this subsection is to discuss the expected quality of the surface wind forecast obtained by dynamic adaptation, and the reasons for relative failure when this happens. The main reasons which can cause a bad surface wind prediction are identified. Every one of them is probable in a mountainous, or otherwise very heterogeneous region.

First, it is expected, confirmed by extensive experimentation, that the method performs better when the wind is stronger, or in general strong enough to attenuate the locally induced circulation due to factors other than dynamic forcing. Here mainly thermal circulation, which could only be predicted by a model running on the scale of the adaptation model and with full or even extended package of physical parameterisations for a longer time, commencing at sunrise, is an example. In fact some Alpine valleys may even be big enough to be resolved at the scale of the driving model (Egger, 1987), but for the mechanism of the thermal wind, smaller side valleys are also important. Moreover, the adaptation time is too short to initialize a thermal circulation for which the usual time scale is about half a day. Of course on the other hand, such thermal circulations exist, which are resolved even in large-scale models, like a sea breeze, for example. Those can be succesfully downscaled using the described method.

In certain situations advection may play a significant role (Fig. 9). When, for example, a well expressed small-scale feature like a lee vortex

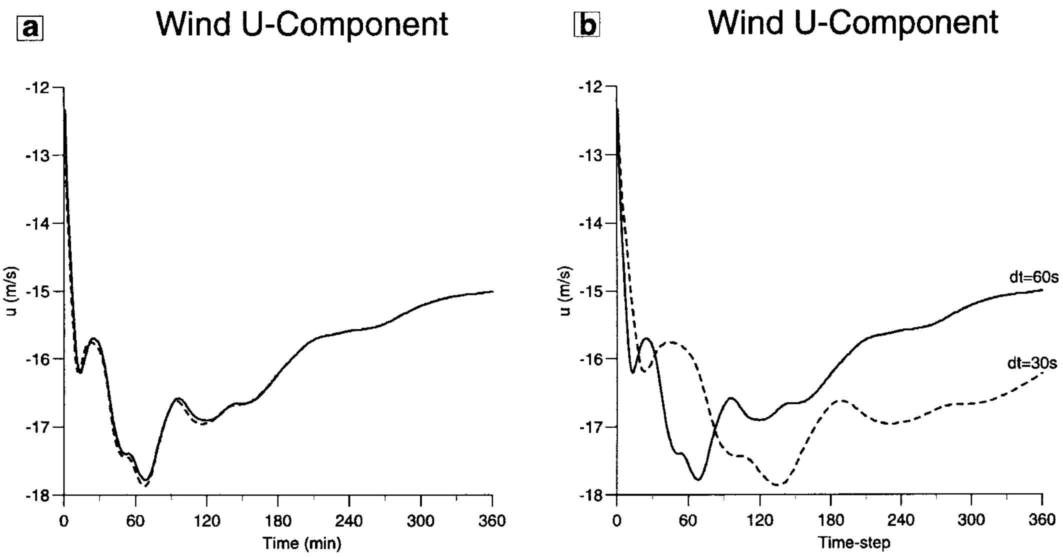

Fig. 8. Time evolution of the u-component of surface wind at another point in the VF configuration. Full line: 60 s time-step; dashed line: 30 s time-step; (a): time on x-axis; (b): time-steps on x-axis.

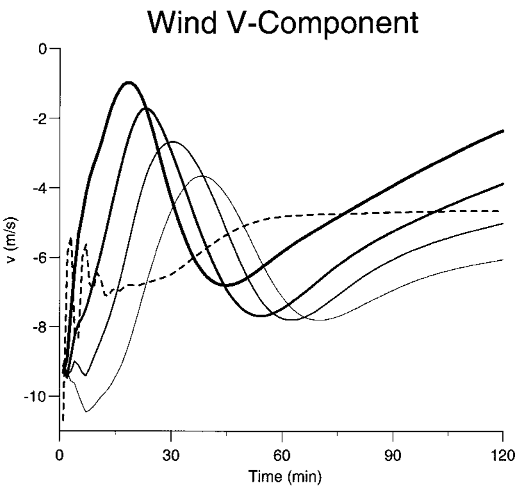

Fig. 9. Time evolution of the v-component of surface wind over 4 successive grid-points downwind (south) of the lee calm (3-D vortex, full lines) and over an arbitrary point (dashed line). Data is from the experiment in the configuration M.

occurs due to dynamic adaptation in favuorable circumstances, this feature may be considered as an atmospheric object and is subjected to advective displacement. In the described case the disturbance connected to the lee phenomenon arrived at the four successive, downwind points with regular delay. The speed of advection can be estimated from Fig. 9; it is equal to about 25 m/s and corresponds to the mean wind above this area at levels between 500 and 850 hPa.

There is always a possibility that the wind forecast of the driving model is missed. In such an unfortunate case, the dynamic adaptation retains this error, or even amplifies it in the areas where the small-scale wind field is very sensitive to the direction of the larger scale flow.

The presence of a temperature inversion in nature, if the driving model does not predict it (which in fact presents another case of a missed forecast in the driving model), will definitely cause a wrong forecast in the adaptation model. The adaptation period is far too short for physical and dynamical processes to create an inversion layer, even if the full physics were included and if a new description of orography would allow it.

5. Conclusions

The main advantage of the method presented is its small computational cost. This means that when a detailed surface wind is the meteorological field of the interest, it is not inevitable to run a model at a very high resolution, with full physical parameterisations and with dense vertical discretisation throughout the atmosphere for a full forecast range. Instead, the described approach may be used, reducing the computational costs by up to and beyond a factor of 100.

The time-scale of adaptation depends on the nature of the desired goal: either an overall wind field of the whole area of interest, or a detailed capture of a specific feature in this field. For general information for the whole area the time needed for adaptation is close to the one estimated by scale analysis at 15 min. By a simple theoretical linear model this time is estimated at around 7 min with a pressure gradient as the prevailing force, and at around 30 min when friction effects prevail. For the adaptation of specific details in the wind field the time needed can be several times longer.

Numerical experiments prove that 30 min of numerical integration of the adaptational model, without previous initialisation, should be sufficient in the majority of cases. This time does not depend on the configuration of the adaptational model as long as the computational domain is big enough, typically 500 km in each direction and even less with very high resolution ($\sim$2.5 km). It was shown that as regards the size of the domain needed for successful adaptation, it is the physical distance which is of the primary importance and not the number of grid-points between the area of interest and the border of the model.

In the scope of the present paper the dynamic adaptation was proved to be a purely dynamic and not a numerical process, and this leads to the assumption that the method is not model-dependent.

Apart from the drawback that the dynamic adaptation with the simplified adapatational model fails in the case of certain atmospheric conditions, such as valley inversion, passage of a cold front, etc., it is probably very useful when there is an instant need for a detailed wind forecast over a limited domain, as for example in the case of sudden pollution, etc.

In future research an evaluation of the reliability of the dynamic adaptation method for small-scale forecasting, depending on the initial weather situation will be made. By adjusting the wind field to more accurate orography the corresponding vertical motion in the vicinity of the surface is also obtained. It will be important to investigate whether this can present a way to use a similar method to that described in this article for predicting some other phenomena, for example the intensity of precipitation on the local scale.

6. Acknowledgements

We wish to thank our colleagues from the Aladin project for the common development of the model, and especially to Jean-François Geleyn for productive advices and guidance, and other colleagues for useful remarks and helping us to improve the English. We appreciate the remarks of two anonymous reviewers; their profound comments resulted in substantial improvement of the paper. Much of this work was accomplished during the stay of the first author at Météo France, CNRM/GMAP. The stay was supported by a scholarship from the French "Ministère de l'Enseignement Supérieur et de la Recherche".

7. Appendix A

Imagine the situation when at time $t = 0$, the vertical wall bounding one side of an infinite tank of water, or a pool of a cool air, of a height $2H$ is removed. The fluid starts to spill and the shallow water equations (with the Coriolis force neglected) can be used to describe the velocity of the flow and the shape of the water surface:

$$\frac{\partial u}{\partial t} = -g\frac{\partial h}{\partial x} - ku, \tag{A.1}$$

$$\frac{\partial h}{\partial t} + H\frac{\partial u}{\partial x} = 0. \tag{A.2}$$

In this system h is the height of the fluid's surface and H is the characteristic depth of the fluid, u is the x-component of velocity, k is the linear friction coefficient, and g is the acceleration due to gravity.

After differentiating eq. (A.1) by x, eq. (A.2) by t and some rearranging, the following characteristic equation can be obtained:

$$\frac{\partial^2 h}{\partial t^2} - gH\frac{\partial^2 h}{\partial x^2} + k\frac{\partial h}{\partial t} = 0. \tag{A.3}$$

We assume the solution of (A.3) to be of the form of a sum of harmonic components:

$$h = \mathrm{Re}[h'] = \mathrm{Re}\sum_n \hat{h}_n\, \mathrm{e}^{-i[(x/L_n)-(t/\tau_n)]} \tag{A.4}$$

where $\hat{h}_n$ are the amplitudes of each of the harmonic components, L_n their characteristic lengths, and τ_n the characteristic time scales of each of the harmonic components.

Substituting such a solution into (A.3) we get the quadratic equation for $1/\tau_n$:

$$-\frac{1}{\tau_n^2}-\frac{ik}{\tau_n}+\frac{gH}{L_n^2}=0$$

$$\Rightarrow \frac{1}{\tau_n}=-\frac{ik}{2}\pm\sqrt{-\frac{k^2}{4}+\frac{gH}{L_n^2}}. \quad (A.5)$$

For further discussion of the contribution of the square root in the last equation to the time scale of the process, the critical length is introduced and the term $-ik/2$ is moved to the front of the parenthesis:

$$\frac{1}{\tau_n}=-\frac{ik}{2}\left[1\mp\sqrt{1-\left(\frac{L_{cr}}{L_n}\right)^2}\right], \quad (A.6)$$

where L_{cr} is the critical length $L_{cr}=2/k\sqrt{gH}$.

The imaginary value of the square root in (A.6) contributes to the harmonic behaviour of $h(x, t)$ in time, while its real value represents the contribution to the time scale of the exponential evolution of the amplitude in time. (In general this is a decrease in the upper part, behind the dam, and an increase of the level in the lower part, below the dam.)

Let L_n and L_{cr} be measured by the characteristic depth of fluid H: $L_n=p_nH$ and $L_{cr}=rH$, where $r=2/k\sqrt{g/H}$. The short notation s_n is used then for the ratio $L_{cr}/L_n=r/p_n\equiv s_n$. With s_n the expression (A.6) shortens to:

$$\frac{1}{\tau_n}=-\frac{ik}{2}(1\mp\sqrt{1-s_n^2}). \quad (A.7)$$

If the same magnitude of friction coefficient is applied as in Section 2, that is $k\sim 5\cdot 10^{-4}\,\mathrm{s}^{-1}$, and if we choose $H\sim 1$ m it follows that $r\sim 10^4$.

As regards the range of useful values of L_n a limitation to the most relevant harmonic components is appropriate: with $0.01H\leq L_n\leqslant 100H$ the level of the fluid can certainly be described in great detail. So the range of values of the ratio $s_n=L_{cr}/L_n$ in the interval $10^2\leqslant s_n\leqslant 10^6$ is certainly wide enough for the considered case.

That means that all relevant values of s_n have a rather high value: at least $s_n\geqslant 10^2$. So the square root in the expression (A.7), for this consideration, is imaginary for all practically important harmonic components: $\sqrt{1-s_n^2}\approx is_n$. The value of the root does not contribute to the time scale of the change of amplitudes of the relevant harmonic components.

Only the factor in front of the parenthesis remains imaginary in (A.7):

$$\frac{1}{\tau_{im}}=-\frac{ik}{2}. \quad (A.8)$$

Only this factor contributes to the time development of the amplitudes of the harmonic components of $h(x, t)$:

$$h=\mathrm{Re}[h']=\mathrm{e}^{-kt/2}\,\mathrm{Re}\sum_n \hat{h}_n\,\mathrm{e}^{-i[(x/L_n)-(t/s_n)]}. \quad (A.9)$$

The time scale of the exponential lowering or rising of the level of fluid on the two sides of the dam is therefore the same for all relevant harmonic components:

$$\mathcal{T}=-im(\tau)=\frac{2}{k}. \quad (A.10)$$

To complete the analysis of the exponential time evolution the scales below the critical length L_{cr} should also be considered. For these, *1* prevails over s_n^2 and the square root has a real value. For these scales dispersion occurs and their time scales differ according to eqs. (A.5) to (A.7).

There are also two asymptotic solutions for $\mathcal{T}$, for the case which is not space-dependent $h=h(t)$, when $L_n\to\infty$, or $s_n\to 0$.

For the time scale then follows the equation

$$\frac{1}{\tau}=-\frac{ik}{2}(1\mp\sqrt{1}), \quad (A.11)$$

which offers two values for the time scale $\mathcal{T}$: $1/k$ and ∞.

The value of $\mathcal{T}=\infty$ represents the case $h(t\to\infty)$, when:

$$h=\mathrm{Re}\sum_n \hat{h}_n\,\mathrm{e}^{-\infty}=\mathrm{Re}\sum_n \hat{h}_n=H. \quad (A.12)$$

This asymptotic solution represents the final state when the fluid is spilt over the whole domain into a layer of uniform depth H.

The second solution is space-independent as well, but retains time-dependence. It can be understood as a general, overall view of the whole spatial domain of the process. For such an overall consideration from (A.11) follows the corresponding value for $\mathscr{T} = 1/k$, leading to the solution:

$$h = \mathrm{e}^{-kt} \operatorname{Re} \sum_n \hat{h}_n. \tag{A.13}$$

For this case, the process is twice as quick as the one for each individual space-dependant harmonic component. Obviously, if the overall, whole-area solution is considered, then the two levels seem to accommodate quicker: the part above the dam falls, the part below the dam rises and so each level accommodates relative to the other twice as quickly as each of the two levels with respect to the solid, steady bottom.

REFERENCES

Davies, H. C. 1976. A lateral boundary formulation for multi-level prediction models. *Quart. J. Roy. Meteorol. Soc.* **102**, 405–418.

Egger, J. 1987. Simple models of the valley-plain circulation. Part I: Minimum resolution model. *Met. Atm. Phys.* **36**, 231–242.

Fox-Rabinovitz, M. S. and Gross, B. D. 1993. Diabatic dynamic initialisation. *Mon. Wea. Rev.* **121**, 549–564.

Fox-Rabinovitz, M. S. 1996. Diabatic dynamic initialisation with an iterative time integration scheme as a filter. *Mon. Wea. Rev.* **124**, 1544–1557.

Gross, G. and Wippermann, F. 1987. Channeling and counter-current in the Upper Rhine valley: numerical simulations. *J. Clim. Appl. Met.* **26**, 1293–1304.

Horányi, A., Ihász, I. and Radnóti, G. 1996. ARPEGE/ALADIN: A numerical weather prediction model for central Europe with the participation of the Hungarian meteorological service. *Időjárás* **100**, 277–301.

Kurihara, Y. and Tuleya, R. E. 1978. A scheme of dynamic initialisation of the boundary layer in a primitive displaymath model. *Mon. Wea. Rev.* **106**, 114–123.

Machenhauer, B. and Haugen, J. E. 1987. Test of spectral limited area shallow water model with time-dependent lateral boundary conditions and combined normal mode/semi-Lagrangian time integration schemes. *ECMWF Workshop Proceedings: Techniques for horizontal discretization in numerical weather prediction models.* Reading, UK, 2–4 November 1987, pp. 361–377.

Majewski, D. 1985. A technique for smooth transformation of large-scale analyses onto a high resolution grid. *ECMWF Workshop on high-resolution analysis.* Reading, UK, 24–26 June 1985, pp. 129–154.

Masson, V. and Bougeault, P. 1996. Numerical simulations of a low-level wind created by complex orography: a Cierro case study. *Mon. Wea. Rev.* **124**, 701–715.

Nickus, U. and Vergeiner, I. 1984. The thermal structure of the Inn valley atmosphere. *Arch. Met. Geoph. Biokl.* **A33**, 199–215.

Pielke, R. A. 1984. *Mesoscale meteorological modelling.* Academic Press, Orlando, USA, XII + 612 pp.

Simmons, A. and Burridge, D. 1981. An energy and angular momentum conserving vertical finite difference scheme and hybrid vertical coordinates. *Mon. Wea. Rev.* **109**, 2003–2012.

Smedman, A.-S., Bergström, H. and Högström, U. 1996. Measured and modelled local wind fields over a frozen lake in a mountainous area. *Beitr. Phys. Atmos.* **69**, 501–516.